Spin-orbit splitting of valence and conduction bands in HgTe quantum wells near the Dirac point

G. M. Minkov,[1] A. V. Germanenko,[1] O. E. Rut,[1] A. A. Sherstobitov,[1,2] M. O. Nestoklon,[3]
S. A. Dvoretski,[4] and N. N. Mikhailov[4]

[1]*Institute of Natural Sciences, Ural Federal University, 620002 Ekaterinburg, Russia*
[2]*M. N. Miheev Institute of Metal Physics of Ural Branch of Russian Academy of Sciences, 620137 Ekaterinburg, Russia*
[3]*Ioffe Physical-Technical Institute, Russian Academy of Sciences, 194021 St. Petersburg, Russia*
[4]*Institute of Semiconductor Physics RAS, 630090 Novosibirsk, Russia*

(Received 14 December 2015; revised manuscript received 20 February 2016; published 11 April 2016)

Energy spectra both of the conduction and valence bands of the HgTe quantum wells with a width close to the Dirac point were studied experimentally. Simultaneous analysis of the Shubnikov–de Haas oscillations and the Hall effect over a wide range of electron and hole densities yields surprising results: the top of the valence band is strongly split by spin-orbit interaction while the splitting of the conduction band is absent, within experimental accuracy. This holds true for the structures with normal and inverted band ordering. The results obtained are inconsistent with the results of *kP* calculations, in which the smooth electric field across the quantum well is only reckoned in. It is shown that taking into account the asymmetry of the quantum-well interfaces within a tight-binding method gives reasonable agreement with the experimental data.

DOI: 10.1103/PhysRevB.93.155304

I. INTRODUCTION

Heightened interest in two-dimensional (2D) structures with quantum wells of gapless semiconductors is caused by the fact that different types of carrier energy spectra could be realized in these structures depending on the width (d) of the quantum well. One of the most intensively studied systems both theoretically and experimentally is the heterostructure with a CdTe/HgTe/CdTe quantum well. The calculations of the energy spectrum in the framework of the *kP* method for symmetrical quantum wells show that there is a critical width of the HgTe quantum well, $d = d_c \simeq 6.3$ nm, when the Dirac-like energy spectrum that is linear in quasimomentum should be realized at small quasimomentum (k) [1,2]. At $d < d_c$, the energy spectrum is normal. The valence band is formed from heavy-hole states while the conduction band is formed from electron states and light-hole states. At $d > d_c$ these states change places, and such a spectrum is called an inverted spectrum. Another approach, namely the calculation in the framework of the tight-binding model, which takes into account the bulk inversion asymmetry of the zinc-blende lattice, yields a similar result regarding the $E(k)$ dependence except that the relatively large anticrossing at $k = 0$ and the large spin-orbit (SO) splitting of the conduction and valence band appear at $d = d_c$ [3].

Knowledge of the energy spectrum is necessary for an understanding of all of the properties of 2D systems, including optical, transport, and others. However, experimental study of the energy spectrum has been rather superficial to date. Comparatively, the energy spectrum of the conduction band has been studied in greater detail [4–8]. It was shown that the SO splitting of the conduction band in technologically symmetric quantum wells does not reveal itself in most cases. The conduction band is not parabolic: the effective mass increases with increasing electron density. These data are in satisfactory agreement with results of theoretical calculations performed in the framework of the *kP* method.

The energy spectrum of the valence band has been investigated somewhat less, and it should be noted that the experimental data are inconsistent with the theoretical results in many cases. For instance, in structures with $d >$ 10 nm, which corresponds to the inverted energy spectrum, the hole effective mass (m_h) obtained experimentally within the wide hole density range $p = (1\text{–}4) \times 10^{11}$ cm^{-2} occurs substantially less than that calculated within the *kP* method: $m_h \simeq (0.15\text{–}0.3)m_0$ [9–11] instead of $(0.5\text{–}0.6)m_0$ [12]. These calculations predict also that the conduction band should overlap with the valence band, the top of which is located at $k \neq 0$ when $d \gtrsim$ (12–15) nm. Although this prediction is in qualitative agreement with the experimental data [11,13], the quantitative difference between theory and experiment is drastic. Experimentally, the top of the valence band is located at $k \simeq 0.5 \times 10^6$ cm^{-1}, while the theoretical prediction gives a value of about $k \simeq 2.5 \times 10^6$ cm^{-1}.

The valence-band spectrum in heterostructures with normal band ordering was explored in only a few studies. The experimental data published in Refs. [14] and [15] for structures with $d = (5\text{–}6)$ nm are very similar, however the interpretation differs significantly. Analyzing the Hall density and the Fourier spectra of the Shubnikov–de Haas (SdH) oscillations, the authors of Ref. [14] were able to describe the data taking into account the secondary maxima of the dispersion law located at $k \neq 0$. But this has been done only for one hole density. Studying analogous heterostructures, the authors of Ref. [15] showed that such an interpretation does not describe the experimental data within a wide hole density range. They showed that all the results are well described under the assumption that the top of the valence band is very strongly split by SO interaction. One possible reason for such splitting is a strong electric field of the *p-n* junction of technological origin in which the quantum well is embedded. The authors were unable to investigate the splitting of the conduction band. These data would make the interpretation more reliable.

In the present paper, we report the results of an experimental study of both hole and electron transport in HgTe quantum wells of different width near the critical point d_c with normal and inverted energy spectra. The measurements were performed over a wide range of carrier density. It

has been found experimentally that the valence band is strongly split by SO interaction, while the conduction band remains unsplit independent of energy-band ordering. We believe that the natural interface inversion asymmetry of zinc-blende heterostructures is responsible for these peculiarities. Quantitatively, the experimental data are well described in the framework of atomistic calculation [3].

II. EXPERIMENT

Our samples with HgTe quantum wells were realized on the basis of HgTe/$Hg_{1-x}Cd_xTe$ ($x = 0.55$–0.65) heterostructures grown by molecular beam epitaxy on GaAs substrate with the (013) surface orientation [16]. A sketch of the structures investigated is shown in the inset of Fig. 2(a). The samples were mesa-etched into standard Hall bars of 0.5 mm width, and the distance between the potential probes was 0.5 mm. To change and control the carrier density in the quantum well, the field-effect transistors were fabricated with parylene as an insulator and aluminum as a gate electrode. For each heterostructure, several samples were fabricated and studied. The measurements were performed at temperatures of 1.3–20 K.

III. CHARACTERIZATION OF SAMPLES REGARDING THE TYPE OF SPECTRUM

To interpret the experimental results, it is very important to know whether the spectrum of the structure under study is normal or inverted. The values of the quantum-well width presented in Table I are nominal, therefore it is very desirable to have independent data on the spectrum type.

The most reliable method to determine the type of spectra can be based on the peculiarity of the spectrum quantization in the external magnetic field. Theoretical calculations [6,12,17] and experimental investigations [11,17] show that there are two anomalous Landau levels, the behavior of which is radically different for the normal and inverted spectra [Figs. 1(c) and 1(f)].

As seen from Fig. 1(f), the Landau levels -2 and 0 for the case of the inverted spectrum start at $B = 0$ from the bottom of the conduction band and the top of the valence band, respectively, and moving toward each other they cross in the magnetic field $B = B_c$. The B_c value depends on the quantum-well width. It increases as d increases, achieves a maximal value of about 9–10 T at $d \simeq (9$–$10)$ nm, and then decreases with a further d increase. In the structures with a normal spectrum, the energy positions of the anomalous Landau levels at $B \to 0$ are opposite: level -2 starts from the valence-band top while level 0 goes from the conduction-band bottom. Because they move in the same directions as for $d > d_c$, the crossing does not occur in this case [Fig. 1(c)]. Thus, if the crossing of Landau levels is detected experimentally, the real width of the HgTe quantum well is greater than the critical value d_c, and the sample under study is in the inverted regime.

When B_c is large enough that the anomalous Landau levels have a large density of states and are well separated, the cross manifests itself as a nonmonotonic peculiarity in the ρ_{xx} versus B and ρ_{xy} versus B dependences [11]. When the quantum-well width is close to the critical value d_c, the cross of the Landau levels occurs at such a low magnetic field that it may not reveal itself in magnetotransport measurements. It is possible in this case to observe the cross by studying the behavior of the quantum capacitance (C_q) in the magnetic field at the gate voltages close to the charge-neutrality point (CNP). Unlike the resistance components, which depend not only on the density of states (ν) but also on the disorder strength, the quantum capacitance depends on the density of states only, $C_q = e^2 dn/d\mu = e^2\,\nu(\mu)$, where μ stands for the chemical potential. Therefore, the value of C_q at $V_g \simeq V_g^{\mathrm{CNP}}$ should increase with growing B, achieve the maximal value at $B = B_c$, and then decrease with the further increase of the magnetic field even when the Landau levels are rather broadened. When the Fermi level is located in the conduction or valence band at $V_g \neq V_g^{\mathrm{CNP}}$, the maximum in the dependence $C_q(B)$ should also be observed, but in the higher magnetic fields as compared with B_c.

In the structures with a normal energy spectrum, the anomalous Landau levels are moving apart and the density of states in the gap (which is nonzero due to smearing) decreases with growing magnetic field. Thus, the capacitance should decrease with B near the CNP.

Measurements of the quantum capacitance were taken for all the structures investigated. In Fig. 2(a) we have presented, as an example, the dependence $C_q(V_g)$ measured at $B = 0$ on the structure 1023. The nonmonotonic volt-capacitance characteristic is a consequence of the nonmonotonic energy dependence of the density of states. The minimum in the vicinity of CNP is observed when the Fermi level goes through the energy gap where the density of states is much smaller than that in the valence and conduction bands.[1] Figure 2(b) shows the magnetic-field dependences of C_q at different V_g near the CNP. The maximum in these curves at $B = B_{\max}$, which shifts to higher B values when V_g deviates from the CNP, is clearly evident. As can be seen from Fig. 2(c), the $B_{\max}$ versus V_g plot has a minimum, and just the minimal value of $B_{\max} \simeq 1.2$ T corresponds to the magnetic field B_c

TABLE I. The parameters of heterostructures under study.

No.	d (nm)	p_s (cm^{-2})	B_c (T)	Q/e (cm^{-2})[a]	p_1/p_2
1122	5.6	1.3×10^{11}		2.5×10^{11}	1.8–2.2
H724	5.8	1.5×10^{11}		1.0×10^{11}	2.0–2.2
1123	6.0	6.0×10^{10}		1.5×10^{11}	2.0–2.3
1121	6.3	8.0×10^{10}	0.6 ± 0.2	7.6×10^{10}	2.2–2.5
1023	6.5	3.6×10^{10}	1.1 ± 0.2	1.0×10^{10}	2.3–2.7
				-7.0×10^{10} [b]	
1022	6.7	1.4×10^{10}	1.2 ± 0.2	1.5×10^{10}	2.3–2.8
				-1.5×10^{10} [b]	
1124	7.1[c]	3.4×10^{10}	~ 0	2.2×10^{11}	2.2–2.8

[a] At $V_g = 0$.
[b] After illumination.
[c] The fact that $B_c \sim 0$ indicates that the real QW width in this structure is close to d_c.

[1] The details of capacitance measurements for HgTe quantum wells of different widths are beyond the scope of this paper and will be published elsewhere.

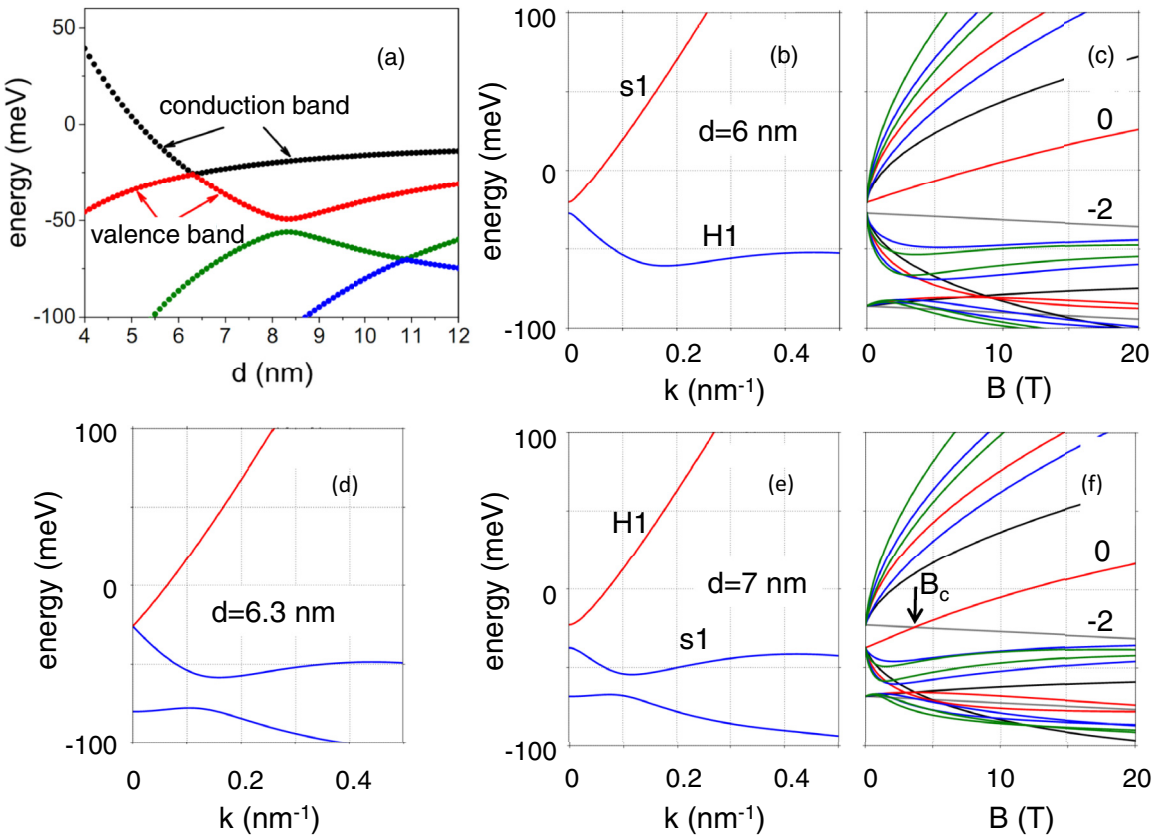

FIG. 1. The spatial quantization subband energies at $k = 0$ plotted against the HgTe quantum-well width (a). The band structure (b),(d),(e) and Landau levels (c),(f) for a quantum well of different widths [12].

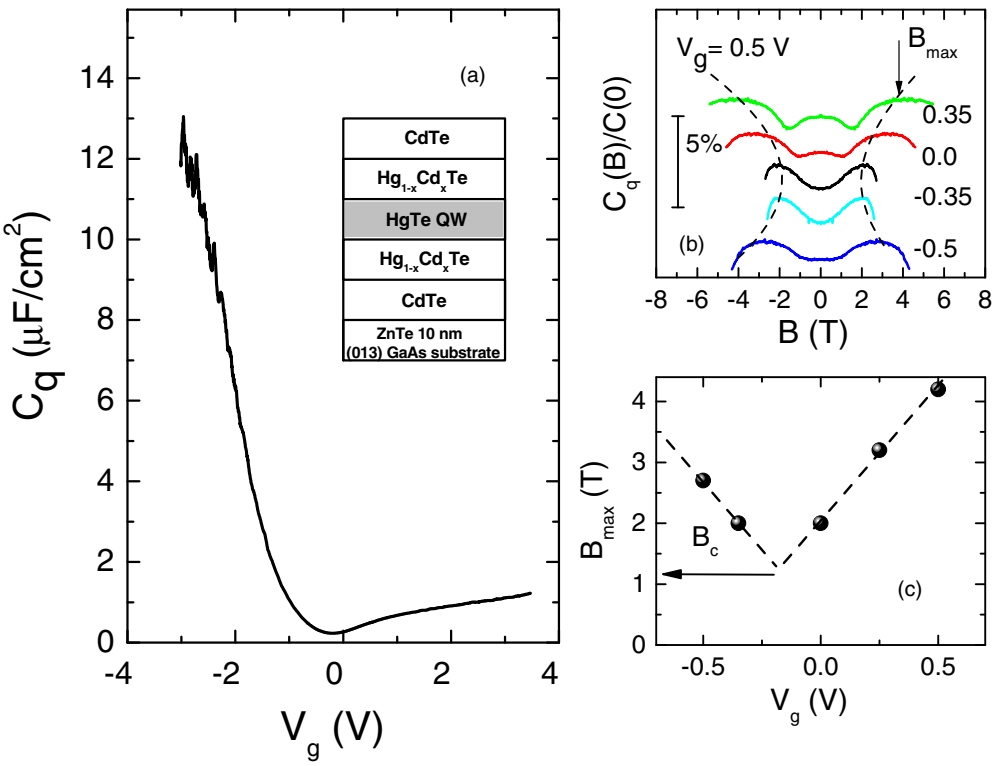

FIG. 2. (a) The gate voltage dependence of the quantum capacitance C_q for the structure 1023 at $T = 4.2$ K and $B = 0$. The inset shows a sketch of the structures under study. (b) The magnetic-field dependences of C_q at the gate voltages close to CNP. (c) The B_{max} values plotted against the gate voltage.

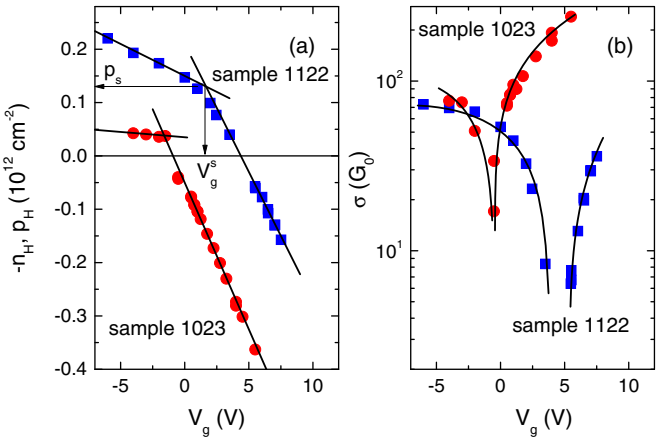

FIG. 3. The gate voltage dependences of (a) the Hall carrier densities $n_{\rm H}$ and $p_{\rm H}$ and (b) the conductivity at $B = 0$ for the structures 1122 and 1023 with $d < d_c$ and $d > d_c$, respectively. $T = 4.2$ K. The lines are provided as a guide to the eye.

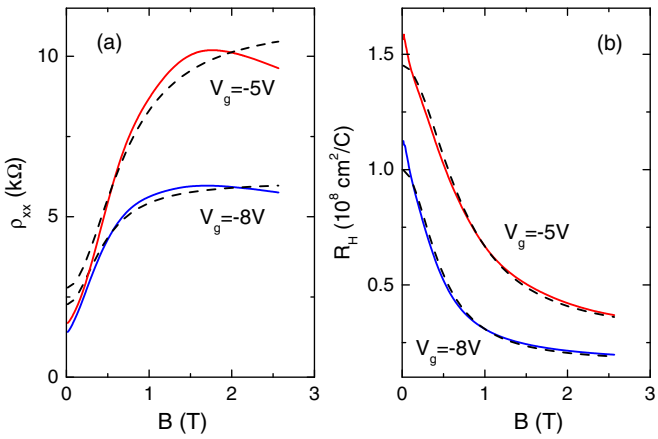

FIG. 4. The magnetic-field dependences of ρ_{xx} (a) and R_H (b) for two gate voltages for the structure 1023, $T = 18$ K. The solid curves are measured experimentally, the dashed ones are the results of the best fit with the parameters shown in Fig. 5.

in which the anomalous Landau levels 0 and -2 cross each other. The analogous maximum in the dependence $C_q(B)$ at V_g close to $V_g^{\rm CNP}$ was also observed in the structures 1022 and 1121. The B_c values obtained in such a manner for these three structures are listed in Table I.

As for the remaining four heterostructures, the quantum capacitance in the vicinity of the CNP decreases as B increases for the structures 1122, H724, and 1123, while for the structure 1124 it is practically independent of B.

Thus the results of capacitance measurements in the presence of a magnetic field show unambiguously that the energy spectrum is inverted in the structures 1022, 1023, and 1121, the structures 1122, H724, and 1123 have normal spectra, while the B independency of quantum capacitance for the structure 1124 indicates that the real width of the quantum well in this structure is close to the critical value, $d \simeq d_c$.

IV. THE VALENCE-BAND SPECTRUM

Let us now inspect the gate voltage dependences of the Hall carrier density obtained at low magnetic field [where $R_H(B)$ is constant] as follows: $n_{\rm H} = -1/eR_H(0.1\ {\rm T})$ when $R_H < 0$ for electron density and $p_{\rm H} = 1/eR_H(0.1\ {\rm T})$ when $R_H > 0$ for hole density. These dependences are plotted in Fig. 3(a) for structures 1122 and 1023 with a normal and an inverted spectrum, respectively. The corresponding V_g dependences of the conductivity are shown in Fig. 3(b). These structures are chosen as typical ones; the results for other structures are analogous. In what follows, we will demonstrate all the results for these structures excepting for the cases when the simultaneous analysis of results for all the structures will be useful. One can see that the electron density depends linearly on V_g over the whole gate voltage range. Note that the slope $dn_{\rm H}/dV_g$ coincides with the value C/eS (where C is the capacitance between the 2D gas and the gate electrode, and S is the gate area[2]), to within experimental error. The hole density changes with the same slope, $dp_{\rm H}/dV_g = -dn_{\rm H}/dV_g$, within a restricted V_g range of only $V_g^s < V_g < {}^{\rm CNP}_g$, where the hole density is less than some critical value $p_s = p(V_g^s)$. For $V_g < V_g^s$, the slope $|dp_{\rm H}/dV_g|$ decreases significantly. An analogous dependence $p(V_g)$ was observed earlier in Refs. [18,19]. As seen from Fig. 3(a), the p_s values are significantly different for these structures: $p_s \simeq 1.3 \times 10^{11}$ cm^{-2} for structure 1122 and $p_s \simeq 0.35 \times 10^{11}$ cm^{-2} for structure 1023. The decrease of $|dp_{\rm H}/dV_g|$ below V_g^s can result from the appearance of a large enough density of states at the Fermi level, which pins it. They can be the states in the secondary maxima of the valence-band spectrum at $k \neq 0$ [see Figs. 1(b), 1(d), and 1(e)] or some states in the barriers or at the interfaces between the layers forming the quantum well.

To understand which of these reasons is the primary one, we analyze the magnetic-field dependences of R_H and ρ_{xx} in classically strong magnetic fields at relatively high temperature at which the SdH oscillations are suppressed. As an example, in Fig. 4 we have presented the ρ_{xx} versus B and R_H versus B plots measured on the structure 1023 at $T = 18$ K for two gate voltages. These dependences are typical for two-type carrier conductivity. The simultaneous fitting of these plots by the standard handbook expression [see, e.g., Ref. [20], Eqs. (8.66) and (8.67)] with use of hole densities $p^{(1)}$ and $p^{(2)}$ and hole mobilities $\mu^{(1)}$ and $\mu^{(2)}$ as the fitting parameters, gives reasonable agreement with the data (see Fig. 4). The hole densities $p^{(1)}$ and $p^{(2)}$ found in this way and the total density $p^{(1)} + p^{(2)}$ together with the hole Hall density $p_{\rm H} = 1/eR_H(0.1\ {\rm T})$ for different V_g values are plotted in Fig. 5(a). It is seen that $p^{(1)}$ is close to $p_{\rm H}$ and the $p^{(1)} + p^{(2)}$ points fall on the straight line, which describes the $n_{\rm H}$ versus V_g data. The values of the mobility of the second type of holes are about (2–3) $\times 10^3$ cm^2/V s [see Fig. 5(b)], which correspond beyond doubt to free carriers.

[2]The capacitance between the 2D gas and the gate electrode can be considered as a constant value in this context because the contribution of the quantum capacitance is less than 1–2 % in the structures under investigation.

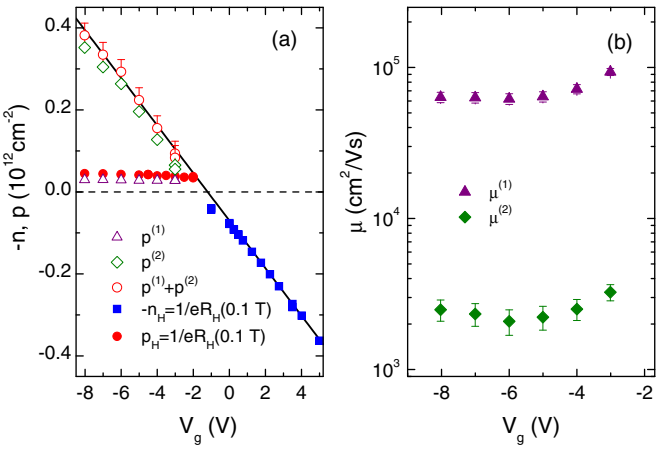

FIG. 5. The gate voltage dependences of the carrier densities (a) and mobilities (b) found from the fit of the magnetic-field dependences of ρ_{xx} and R_H shown in Fig. 4. The solid line is the total charge density (in units of e) in the quantum well found as $Q = C(V_g - V_g^{\mathrm{CNP}})$.

Thus, one can argue that the decrease of $|dp_{\mathrm{H}}/dV_g|$ at $V_g < V_g^s$ is a result of the occupation of the secondary maxima of the valence band when the Fermi level approaches them with decreasing gate voltage. For this case, the value of p_s should depend monotonically on the quantum-well width. To compare the data obtained for the different structures with a different carrier density at $V_g = 0$, a different insulator thickness, and hence a different dn/dV_g value, we have plotted in Fig. 6(a) the values of the Hall carrier densities $1/eR_H(0.1\ \mathrm{T})$ against the total charge in the quantum well $Q = C(V_g - V_g^{\mathrm{CNP}})$ for all the structures investigated. The p_s values found from Fig. 6(a) are plotted against the nominal quantum-well width in Fig. 6(b). The corresponding theoretical dependence calculated within the framework of the 8×8 Kane model in Ref. [12] is presented also. Taking into account the uncertainty

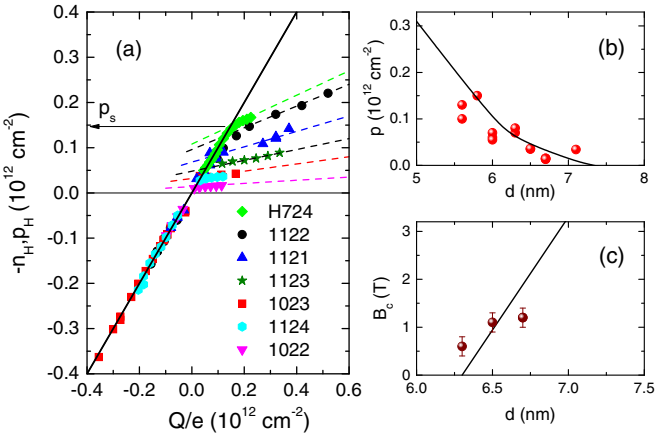

FIG. 6. (a) The Hall carrier density plotted against the charge in the quantum well. As an example, the arrow shows how the p_s value is found for sample H724. The solid line is the carrier density Q/e. The dashed lines are provided as a guide for the eye. The values of p_s (b) and B_c (c) plotted against the nominal quantum-well width. Symbols are the data, while the lines are theoretical results [12].

in the real quantum-well width and the error in the p_s determination, it can be concluded that the value of p_s can be used to estimate the quantum-well width. Note that the experimental values of B_c are also in satisfactory agreement with the calculation results, as is evident from Fig. 6(c).

Before closing this section, let us discuss the specific feature in the behavior of the hole density evident at $p > p_s$. As seen from Fig. 6(a), the higher the p_s value is, the larger is the slope of the dependence $p_{\mathrm{H}}(Q)$ at $p_{\mathrm{H}} > p_s$. Since the Hall coefficient $R_H(0.1\ \mathrm{T})$ gives the density of holes only in the central maximum, the slope of the dependence $p_{\mathrm{H}}(Q)$ at $p_{\mathrm{H}} > p_s$ is determined by the relation between the densities of hole states in the central and secondary maxima ν_1 and ν_2, respectively: $edp_{\mathrm{H}}/dQ = 1/(1 + \nu_2/\nu_1)$. Thus, the increase of dp_{H}/dQ with growing p_s is in qualitative agreement with the fact that the density of states in the central maximum ν_1 at the energy of the secondary maximum increases with the energy increase due to the nonparabolicity of dispersion law $E(k)$.

V. SPIN-ORBIT SPLITTING OF VALENCE AND CONDUCTION BANDS

Now let us turn to a more detailed study of the band spectra. To do this, we have measured the SdH oscillations and their angle dependence over a wide carrier density range.

A. Normal band ordering

1. Valence band

Qualitatively, the results obtained for structures 1122 and their interpretation are analogous to those published in Ref. [15]. Nonetheless, we briefly describe the key results that are important for the interpretation of results both for valence and conduction bands for structures with normal and inverted spectra. The gate voltage dependence of the carrier density, the dependences $\rho_{xx}(B)$ and $d\rho_{xx}(B)/dB$ taken for the structure 1122 at $Q/e = 1.3 \times 10^{11}\ \mathrm{cm}^{-2}$, and the corresponding Fourier spectrum of the SdH oscillations are presented in Fig. 7.

As can be seen from Fig. 7(c), two maxima with frequencies f_1 and f_2 are easily detected in the Fourier spectrum. It is noteworthy that the ratio of the frequencies is close to 2, i.e., the Fourier spectrum is similar to the case when the spin splitting of the Landau levels manifests itself with the magnetic-field increase. In such a situation, the carrier density should be determined as $p_{\mathrm{SdH}} = f_1 \times 2e/h$. Therefore, we obtain $p_{\mathrm{SdH}} = (0.88 \pm 0.05) \times 10^{11}\ \mathrm{cm}^{-2}$ for this concrete case. However, the Hall density at this Q value is significantly larger, $p_{\mathrm{H}} = 1.31 \times 10^{11}\ \mathrm{cm}^{-2}$, as seen from Fig. 7(a).

Such a difference between the hole density found from the SdH oscillations within the proposed model and the hole density found from the Hall effect takes place over the entire hole density range in all the structures investigated. Thus the interpretation described above is invalid for this case.

The only interpretation that adequately describes our results is as follows. Each peak in the Fourier spectrum corresponds to the subband H1, which is strongly split by SO interaction into two subbands H1+ and H1−. In this case the "spin" degeneracy is lifted, and hence the hole densities should be

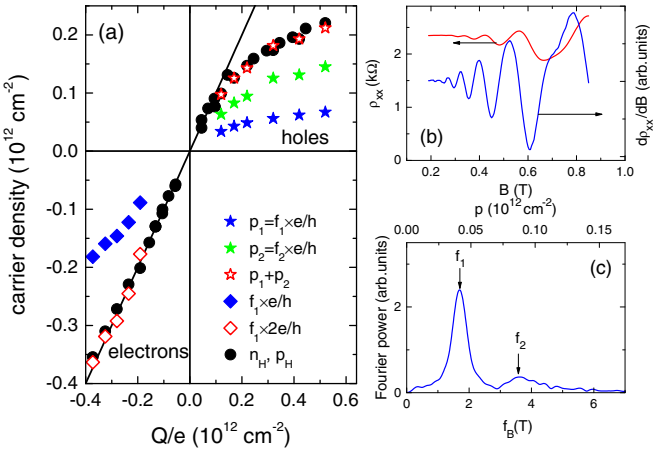

FIG. 7. (a) The carrier density plotted against the charge in the quantum well. The circles are the Hall carrier density, while the stars and diamonds are the carrier densities obtained from analysis of the SdH oscillations as described in the text. The line is the carrier density Q/e. (b) ρ_{xx} and $d\rho_{xx}/dB$ plotted as a function of magnetic field for $Q/e = 1.3 \times 10^{11}$ cm^{-2}. (c) The result of the Fourier transformation of the SdH oscillations of $d\rho_{xx}/dB$ shown in panel (b). Structure 1122.

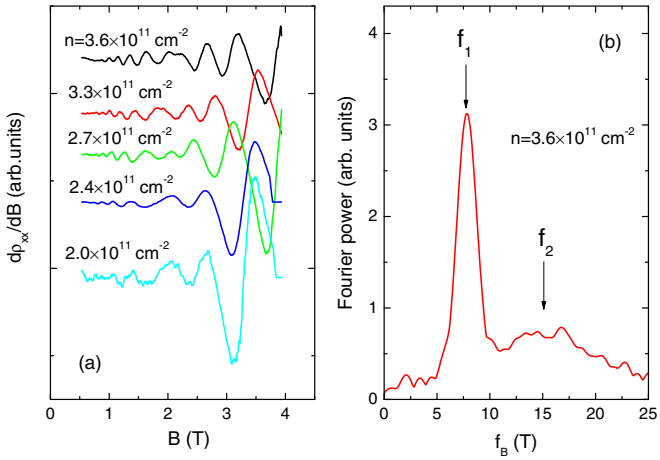

FIG. 8. The SdH oscillations of electron conductivity measured for structure 1122 at different electron densities (a) and the results of Fourier transformation of SdH oscillations for $n = 3.6 \times 10^{11}$ cm^{-2} (b).

found as $p_{1,2} = f_{1,2} \times e/h$, where indexes 1 and 2 correspond to H1+ and H1− subbands. Therefore, the total hole density is $p_{\mathrm{SdH}} = p_1 + p_2 = (f_1 + f_2)\, e/h$. The results of such a data interpretation are represented by stars in Fig. 7(a) within the entire hole density range. One can see that p_{SdH} coincides with p_{H} within experimental error. Thus, we conclude that the valence band is strongly split by SO interaction so that the ratio of hole densities in the split subbands is about 2 over the entire hole density range.

2. *Conduction band*

To obtain the information on the energy spectrum and splitting of the conduction band, we have thoroughly studied the electron SdH oscillations.[3] In Fig. 8(a) we present the SdH oscillations for some Hall densities, and in Fig. 8(b), as an example, we present the Fourier spectrum for one of them. As seen from Fig. 8(b) the Fourier spectrum consists of two peaks whose characteristic frequencies differ by a factor of 2 analogously to the case of the hole conductivity [see Fig. 7(c)]. The main contribution to the peak with the frequency f_1 comes from the low-field SdH oscillations. Therewith, unlike the oscillations in the hole domain, the electron density found as $n_{\mathrm{SdH}} = f_1 \times 2e/h$ is very close to the Hall density, as is evident from Fig. 7(a), indicating that the Zeeman splitting is not resolved. The peak f_2 comes from the oscillations in the high magnetic fields, and it originates from the spin-split Landau levels. This corresponds to the case when the SO splitting of the conduction band is small enough.

[3]Due to large noisiness at positive gate voltage, we could not do this in our previous paper [15]. The possible reason for the noise may be the large resistance of the *p-n* junctions, which are formed in the 2D gas under the gate electrode edge, because these structures are of *p* type at $V_g = 0$.

Thus, the analysis of SdH oscillations carried out over the whole carrier density range gives a surprising result: the valence band is strongly split by SO interaction, while the splitting of the conduction band in the same structure does not reveal itself.

3. *The Shubnikov–de Haas effect in a tilted magnetic field*

To ensure that our interpretation is correct, one can explore the SdH oscillations in a tilted magnetic field. Really, when the SO splitting is significantly smaller than the Zeeman energy ($\Delta_{\mathrm{SO}} \ll \mathrm{g}\mu_B B$), the energy of orbital quantization depends on the normal component of the magnetic field $B_\perp = B\cos\theta$, where θ is the angle between the magnetic-field direction and the normal to the 2D gas plane, while the energy of spin splitting depends on total B. At low magnetic field, where the SdH oscillations are unsplit, this should manifest itself as a strong angle dependence of the oscillation amplitude. In the opposite case of a strong spin-orbit SO interaction ($\Delta_{\mathrm{SO}} \gg \mathrm{g}\mu_B B$), the spin is rigidly coupled with the orbital motion, and the SdH oscillations should be determined by the normal component of the magnetic field only.

The oscillations of $d\rho_{xx}/dB_\perp$ at $B_\perp < 1.2$ T for the electron density 2.5×10^{11} cm^{-2} for several tilt angles are presented in Fig. 9(a). The oscillations within this magnetic-field range are caused by unsplit Landau levels. It is seen that the oscillations decrease in amplitude when B deviates from the normal orientation, practically disappearing at $B_\perp/B \simeq 0.6$, and then they change phase and increase in amplitude upon a further decrease of the $B_\perp$-to-B ratio. This behavior results from the change of the ratio between the spin and cyclotron energies $X = \mathrm{g}\mu_B B/\hbar\omega_c$ with a tilt angle. If $\mathrm{g}\mu_B B$ and $\hbar\omega_c$ are proportional to the total magnetic field and the normal component of B, respectively, one can obtain the following expression for the angle dependence of the oscillation amplitude:

$$\frac{A(B_\perp/B)}{A(1)} = \cos\left(\pi X \frac{B}{B_\perp}\right) \Big/ \cos(\pi X). \qquad (1)$$

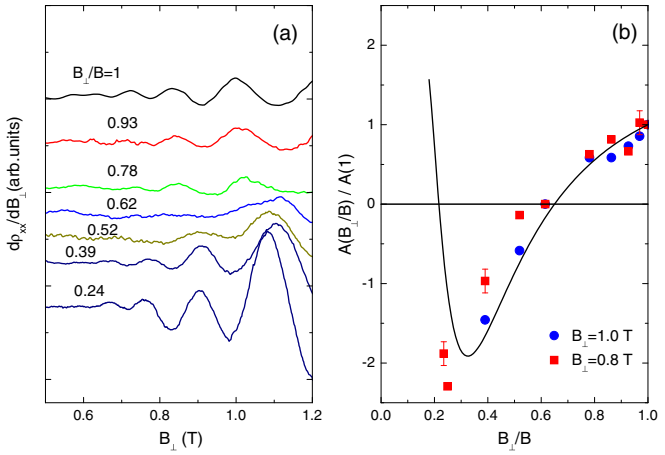

FIG. 9. The SdH oscillations of electron conductivity for structure 1122 at different $B_\perp/B$ values (a) and the oscillation amplitude plotted against the $B_\perp$ to B ratio for $B_\perp = 0.8$ and 1.0 T (b), $n = 2.5 \times 10^{11}$ cm^{-2}. The solid line in (b) is the dependence Eq. (1) with $X = 0.32$. The inversion of the amplitude sign corresponds to the change of the oscillation phase on π.

This dependence together with experimental data are shown in Fig. 9(b). One can see that good agreement is observed when $X = 0.32$.

Let us now inspect the behavior of the SdH oscillations with the changing tilt angle measured on the same heterostructure in the hole domain (Fig. 10). One can see that, unlike the case of electron conductivity, the SdH oscillations plotted against the normal component of the magnetic field remain practically unchanged with the changing tilt angle. This means that they are determined by the normal components of the magnetic field only. As discussed above, such a behavior should be observed when SO interaction is relatively strong: the SO splitting is much greater than the Zeeman energy. Or, alternatively, the independence of the oscillation picture on the tilt angle may be caused as well by a strong anisotropy of the effective g-factor when the in-plane g-factor is much smaller than the perpendicular one, $g_\parallel \ll g_\perp$. However, the estimation made

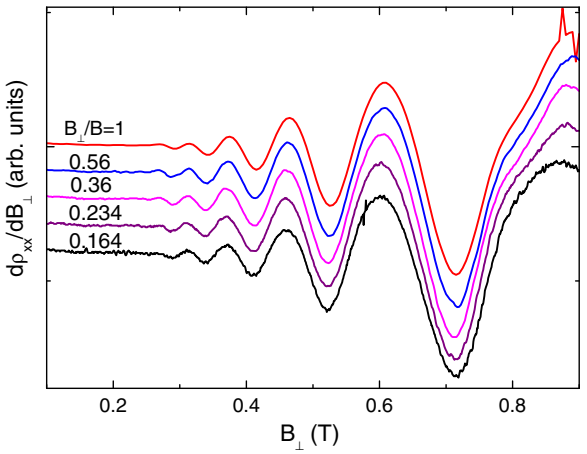

FIG. 10. The SdH oscillations of the hole conductivity plotted against the normal component of magnetic field for structure H1122 at different angles, $p = 1.35 \times 10^{11}$ cm^{-2}.

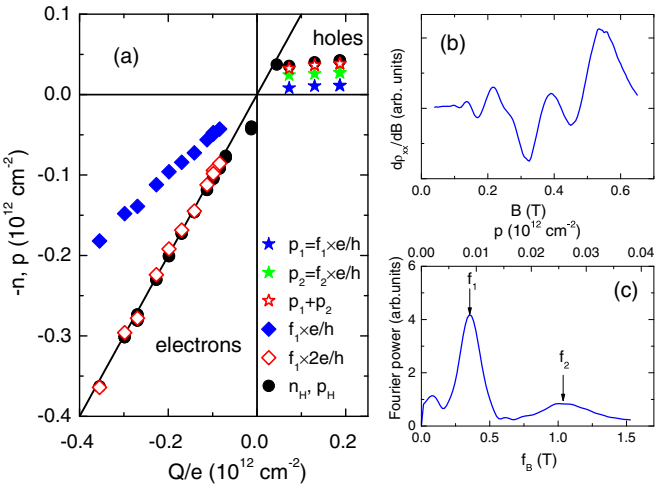

FIG. 11. Results analogous to those presented in Fig. 7, but for structure 1023 with the inverted spectrum.

with the use of Eq. (35) from Ref. [21] shows that this is not the case. The Zeeman splitting differs in the perpendicular and longitudinal orientations of the magnetic field only slightly for the actual quantum-well widths and actual Fermi energies.

Thus, the analysis of the angle dependences of SdH oscillations also shows that the valence-band spectrum is strongly split due to spin-orbit interaction, while the conduction band remains unsplit.

B. Inverted band ordering

The dependence of carrier densities found from the Hall and Shubnikov–de Haas effects on the charge of 2D gas for structure 1023 with an inverted spectrum, $d = 6.5$ nm, is plotted in Fig. 11(a). In general, it is similar to that for the structure with a normal spectrum except that the p_s value is significantly less in structures with $d > d_c$: namely, $p_s \simeq 3.0 \times 10^{10}$ cm^{-2} for structure 1023 instead of $\simeq 1 \times 10^{11}$ cm^{-2} for structure 1122 with a normal spectrum. As discussed in Sec. IV, this results from the smaller energy distance between the top of the valence band at $k = 0$ and the secondary maxima at $k \neq 0$.

The SdH oscillations in the hole conductivity regime and their Fourier spectrum are shown in Figs. 11(b) and 11(c), respectively. As in the structures with a normal spectrum, the only way to reconcile the Hall density and data obtained from the SdH oscillations is to assume that each maximum in the Fourier spectrum is associated with the split subband.

In the electron conductivity regime, the SdH oscillations measured at different tilt angles are presented in Fig. 12(a) for the Hall density $n_H = 1.7 \times 10^{11}$ cm^{-2}. The Fourier spectrum of the oscillations at normal B orientation is shown in the inset of Fig. 12(a).

The charge dependences of the electron densities found as $f_1 \times 2e/h$ and $f_1 \times e/h$ are shown in Fig. 11(a). It is seen that $n_{\mathrm{SdH}} = f_1 \times 2e/h$ coincides with n_H. This means that each peak of the SdH oscillations corresponds to the twofold-degenerate Landau level. As Fig. 11(a) shows, such a coincidence is observed over the whole range of the electron density. Thus, the spin-orbit splitting of the conduction band in

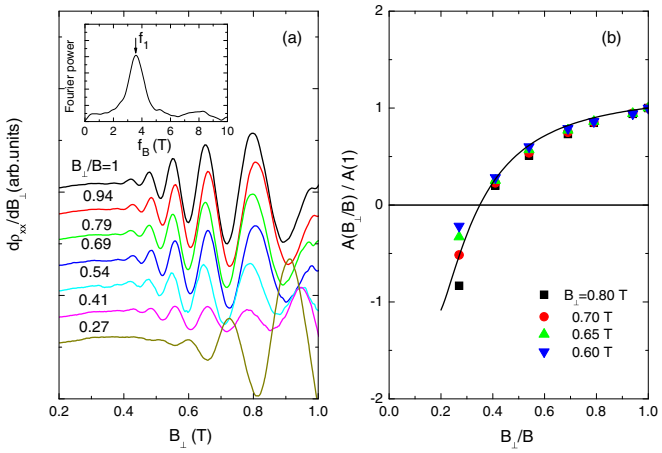

FIG. 12. The SdH oscillations of electron conductivity measured for structure 1023 at different angles (a) and the oscillation amplitude plotted against the $B_\perp$ to B ratio for four $B_\perp$ values (b), $n = 1.7 \times 10^{11}$ cm^{-2}. The solid line in (b) is the dependence Eq. (1) with $X = 0.18$. The inset in (a) is the Fourier spectrum for $B_\perp/B = 1$.

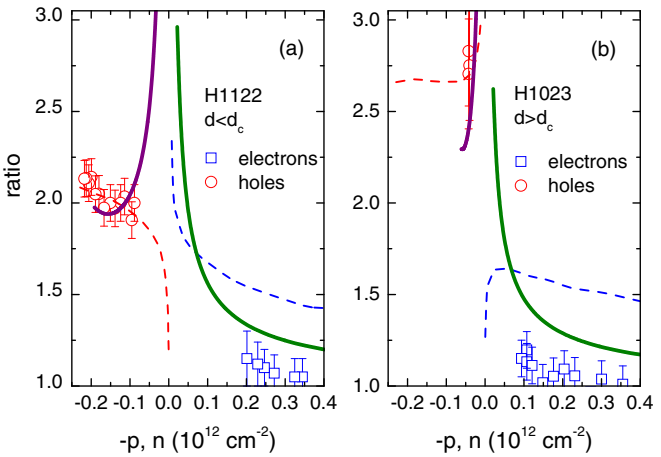

FIG. 14. The ratio between carrier densities in split subbands plotted against the carrier density for structures 1122 (a) and 1023 (b) with normal and inverted spectra, respectively. Symbols are the experimental results, the dashed lines are the results of the kP calculations described in the text, and the solid lines are the results obtained by the sp^3 tight-binding method [3].

the structures with the inverted spectrum does not reveal itself as well as it does in the structures with the normal spectrum.

The conclusion about strong splitting of the valence band and weak splitting of the conduction band is consistent with the behavior of the oscillations in a tilted magnetic field. The behavior of the oscillations of the electron conductivity with the tilt angle shown in Fig. 12(a) is analogous to that presented in Fig. 9(a) for the structure with a normal spectrum. The angle dependence of the oscillation amplitude in Fig. 12(b) demonstrates that the Zeeman splitting becomes equal to half the orbital one at $B_\perp/B$ close to 0.35. The dependence calculated from Eq. (1) with $X = 0.18$ well describes the data.[4]

The SdH oscillations of the hole conductivity measured at a different tilt angle are presented in Fig. 13. As for the structures with the normal spectrum (see Fig. 10), neither positions nor amplitudes depend on the tilt angle that corresponds to strong SO splitting of the valence band (see the discussion above).

Summing up all the data given above, we can formulate the main outcome. The analysis of the Shubnikov–de Haas and Hall effects over the whole carrier density range in the structures with $d < d_c$ and $d > d_c$ gives a surprising result: the valence band is strongly split by SO interaction in the structures both with a normal and an inverted spectrum, while the splitting of the conduction band in the same structures does not reveal itself. To illustrate this, we have plotted the ratio between the carrier densities in the split subbands in the valence and conduction bands as a function of carrier density in Fig. 14.[5] This figure is the key result of the paper.

[4]A detailed analysis of the electron-density dependence of the g-factor in structures with quantum wells of different width is beyond the scope of this study and will be discussed in another paper.

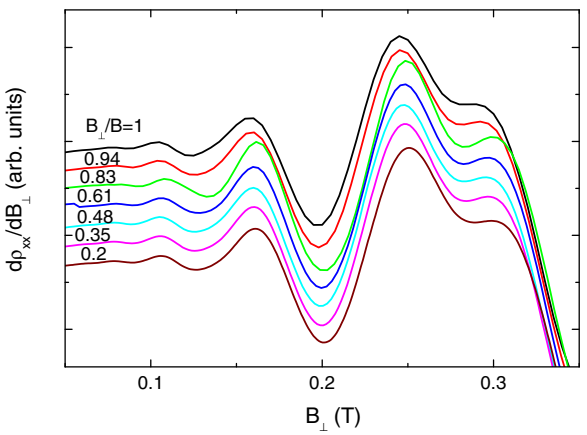

FIG. 13. The SdH oscillations of hole conductivity measured at different angles for structure H1023 with the inverted spectrum, $p = 3.8 \times 10^{10}$ cm^{-2}.

VI. COMPARISON WITH THE RESULTS OF kP AND TIGHT-BINDING CALCULATIONS

The strong SO splitting of the valence band at $d < d_c$ was observed in our previous paper [15]. The experimental results are interpreted under the assumption that the quantum well is located in the strong electric field of a p-n junction, which in turn results in a strong Bychkov-Rashba effect. It has been shown that the kP model describes the valence-band spectrum quantitatively. As noted above, we were unable in that paper to study the conduction band with the accuracy needed to obtain the SO splitting reliably, for heterostructures studied in the present paper it was possible.

Let us first compare the experimental results obtained in the present paper both for the valence and conduction bands with the results calculated within the framework of the kP model used in Ref. [15]. As before, we use here the six-band

[5]We have plotted the ratio p_2/p_1 but not the value of SO splitting, Δ_{SO}, because to calculate Δ_{SO} from p_2/p_1, one needs the carrier effective mass, which is known with some error.

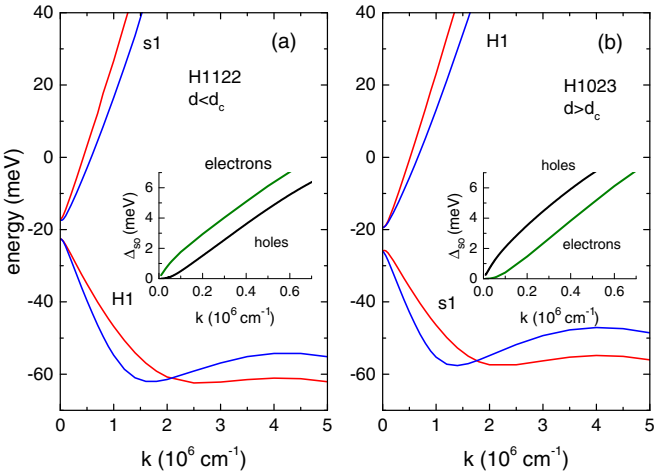

FIG. 15. The dispersion $E(k)$ for structures 1122 (a) and 1023 (b) with normal and inverted spectra, respectively, calculated within the six-band Kane model in the presence of electric field 80 mV/d. In the insets, the SO splitting is plotted against the quasimomentum value.

Kane Hamiltonian. The direct integration technique is applied to solve the Shrödinger equation as described in Ref. [22]. The other parameters were the same as in Refs. [23,24]. As in the previous paper [15], the value of the electric field serves as the fitting parameter, which provides the ratio between the hole densities in the split subbands, which is observed experimentally (see Fig. 14). It is approximately equal to 80 mV/d for all the structures under study.

Let us now inspect the SO splitting of the conduction band. The calculated energy spectrum for the heterostructures with $d < d_c$ and $d > d_c$ is shown in Fig. 15. The energy splitting Δ_{SO} as a function of the quasimomentum value is shown in the insets. It is seen that the splitting of the conduction band at low k values, $k < 0.1 \times 10^6$ cm^{-1}, is much larger than that of the valence band for $d < d_c$. For $d > d_c$, the situation is opposite; the valence band is split much stronger than the conduction band. Such relationships between splittings agree with the known result of symmetry analysis according to which $\Delta_{SO} \propto k$ for the s1 band and $\Delta_{SO} \propto k^3$ for the H1 band near $k = 0$. It should be emphasized that such low quasimomentum values correspond to very low carrier densities ($\sim 10^9$ cm^{-2} and less), which are inaccessible experimentally. At larger quasimomentum values, these relationships are violated. The splitting values of s1 and H1 bands become close to each other. As seen from Fig. 15, the difference in the spin-orbit splitting for the valence and conduction bands does not exceed 30% for both heterostructures for $k_F > 0.5 \times 10^6$ cm^{-1}, which corresponds to the actual carrier density range $n, p > 5 \times 10^{10}$ cm^{-2} (see Fig. 14).

To compare the results of the kP calculations with the experimental data, we have calculated the carrier density in the split subbands as $k^2/(4\pi)$, and we plotted the n_2-to-n_1 and p_2-to-p_1 ratios against the total carrier density in Fig. 14 by the dashed lines. It is evident that this model perfectly describes the data relating to the hole split subband and gives no agreement with the experimental results concerning the conduction-band splitting. One of the reasons why the used kP model fails when compared with the experiment is the fact that it ignores the asymmetry caused by the difference in the quantum-well interfaces.

The role of the bulk inversion asymmetry of host crystals and interface inversion asymmetry in the SO splitting of the energy spectrum of 2D carriers was recently studied in Ref. [3]. Using symmetry analysis and atomistic calculations, the authors obtained a surprising result. The asymmetry of CdTe/HgTe and HgTe/CdTe interfaces forming the CdTe/HgTe/CdTe quantum well results in the giant splitting of the energy spectrum; in the quantum wells of critical and close-to-critical width, $d \simeq d_c$, the splitting reaches a value of about 15 meV.

Analogous calculations have been performed for our concrete case of (013) HgTe quantum wells.[6] The quantum well was supposed symmetric in the sense that no electric field was applied across the well. The microscopic strain has been calculated in the atomistic valence force field model [25] and then incorporated in tight binding using the standard procedure [26]. The tight-binding parameters used in the calculations were obtained using a procedure similar to that described in detail in the supplemental material to Ref. [3] with the following modification. In Ref. [3] it was assumed that the change of the ionicity across the interface may be extracted from the atomic levels obtained in *ab initio* calculations. Instead, one may introduce more physical parameter, the change of the electrostatic potential on anion across the interface, and fit this parameter to reproduce the expected properties of the interface. Tight-binding parameters in Ref. [3] correspond to the change of electrostatic potential on Te between the quantum well and barrier equal to 1 eV, which is in accordance with *ab initio* calculations of the HgTe/CdTe heteropair. For the interface between HgTe and the $Hg_{1-x}Cd_xTe$ ($x \simeq 0.5$) alloy, this parameter should be reduced to 500 meV, which leads to a proportional reduction of the interface-induced spin splitting. The carrier densities in the subbands were calculated as $S_k/(2\pi)^2$, where S_k is the area inside the Fermi contour, which is not a circle due to the absence of axial symmetry. The results of calculations are depicted in Fig. 14 by solid lines. One can see that the atomistic calculations describe the experimental SO splitting of the spectrum reasonably not only for the valence band but for the conduction band also. It is necessary to stress that no fitting parameters have been used in the calculations.

VII. CONCLUSION

We have studied the energy spectrum of the conduction and valence bands of 2D states in HgTe quantum wells by means of magnetotransport measurements. The structures investigated have the width of the quantum wells close to the critical value $d \simeq d_c$, where the spectrum changes from normal (at $d < d_c$) to inverted (at $d > d_c$). Simultaneous analysis of the SdH oscillations and the Hall effect over the wide range of the electron and hole densities yields a surprising result: the top of the valence band is strongly split by spin-orbit interaction

[6]Detailed theoretical analysis in the framework of the tight-binding method is a topic of another paper that is currently in progress.

while the splitting of the conduction band is absent, within experimental accuracy. This conclusion is supported by the results obtained in the tilted magnetic fields. The behavior of the SdH oscillations of electron conductivity with the changing tilt angle corresponds to the case when the orbital quantization is determined by the normal component of the magnetic field, while the spin splitting is determined by the total field. The oscillations of the hole conductivity are totally determined by the normal component of the magnetic field, indicating the SO interaction wins the Zeeman effect in the actual magnetic-field range. Surprisingly, such a ratio of the splittings is observed for structures with a normal spectrum ($d < d_c$) as well as for structures with an inverted one ($d > d_c$). These data are inconsistent with the kP calculations, which take into account the Bychkov-Rashba effect caused by an electric field directed across the quantum well. It is shown that the experimental results can be reasonably described within the framework of the tight-binding method, which properly takes into consideration the interface inversion asymmetry.

ACKNOWLEDGMENTS

We are grateful to I. V. Gornyi, S. A. Tarasenko, and O. E. Raichev for useful discussions. The work has been supported in part by the Russian Foundation for Basic Research (Grants No. 15-02-02072 and No. 16-02-00516) and by Act 211 Government of the Russian Federation, Agreement No. 02.A03.21.0006. A.V.G. and O.E.R. gratefully acknowledge financial support from the Ministry of Education and Science of the Russian Federation under Projects No. 3.571.2014/K and No. 2457.

[1] L. G. Gerchikov and A. Subashiev, Phys. Status Solidi B **160**, 443 (1990).
[2] B. A. Bernevig, T. L. Hughes, and S.-C. Zhang, Science **314**, 1757 (2006).
[3] S. A. Tarasenko, M. V. Durnev, M. O. Nestoklon, E. L. Ivchenko, J.-W. Luo, and A. Zunger, Phys. Rev. B **91**, 081302 (2015).
[4] M. M Schultz, F. Heinrichs, U. Merkt, T. Colin, T. Skauli, and S. Løvold, Semicond. Sci. Technol. **11**, 1168 (1996).
[5] A. Pfeuffer-Jeschke, F. Goschenhofer, S. J. Cheng, V. Latussek, J. Gerschütz, C. R. Becker, R. R. Gerhardts, and G. Landwehr, Physica B **256-258**, 486 (1998).
[6] M. Schultz, U. Merkt, A. Sonntag, U. Rössler, R. Winkler, T. Colin, P. Helgesen, T. Skauli, and S. Løvold, Phys. Rev. B **57**, 14772 (1998).
[7] X. C. Zhang, K. Ortner, A. Pfeuffer-Jeschke, C. R. Becker, and G. Landwehr, Phys. Rev. B **69**, 115340 (2004).
[8] A. V. Ikonnikov, M. S. Zholudev, K. E. Spirin, A. A. Lastovkin, K. V. Maremyanin, V. Y. Aleshkin, V. I. Gavrilenko, O. Drachenko, M. Helm, J. Wosnitza, M. Goiran, N. N. Mikhailov, S. Dvoretskii, F. Teppe, N. Diakonova, C. Consejo, B. Chenaud, and W. Knap, Semicond. Sci. Technol **26**, 125011 (2011).
[9] D. A. Kozlov, Z. D. Kvon, N. N. Mikhailov, S. A. Dvoretskii, and J. C. Portal, Pis'ma Zh. Eksp. Teor. Fiz. **93**, 186 (2011) [JETP Lett. **93**, 170 (2011)].
[10] Z. D. Kvon, S. N. Danilov, D. A. Kozlov, C. Zoth, N. N. Mikhailov, S. A. Dvoretskii, and S. D. Ganichev, Pis'ma Zh. Eksp. Teor. Fiz. **94**, 895 (2011) [JETP Lett. **94**, 816 (2011)].
[11] G. M. Minkov, A. V. Germanenko, O. E. Rut, A. A. Sherstobitov, S. A. Dvoretski, and N. N. Mikhailov, Phys. Rev. B **88**, 155306 (2013).
[12] M. Zholudev, Ph.D. thesis, University Montpellier 2, 2013.
[13] E. Olshanetsky, Z. Kvon, N. Mikhailov, E. Novik, I. Parma, and S. Dvoretsky, Solid State Commun. **152**, 265 (2012).
[14] K. Ortner, X. C. Zhang, A. Pfeuffer-Jeschke, C. R. Becker, G. Landwehr, and L. W. Molenkamp, Phys. Rev. B **66**, 075322 (2002).
[15] G. M. Minkov, A. V. Germanenko, O. E. Rut, A. A. Sherstobitov, S. A. Dvoretski, and N. N. Mikhailov, Phys. Rev. B **89**, 165311 (2014).
[16] N. N. Mikhailov, R. N. Smirnov, S. A. Dvoretsky, Y. G. Sidorov, V. A. Shvets, E. V. Spesivtsev, and S. V. Rykhlitski, Int. J. Nanotechnol. **3**, 120 (2006).
[17] M. König, S. Wiedmann, C. Brüne, A. Roth, H. Buhmann, L. W. Molenkamp, X.-L. Qi, and S.-C. Zhang, Science **318**, 766 (2007).
[18] D. Kozlov, Z. Kvon, N. Mikhailov, and S. Dvoretsky, Pis'ma Zh. Eksp. Teor. Fiz. **96**, 815 (2012) [JETP Lett. **96**, 730 (2012)].
[19] G. M. Minkov, A. V. Germanenko, O. E. Rut, A. A. Sherstobitov, S. A. Dvoretski, and N. N. Mikhailov, Phys. Rev. B **91**, 205302 (2015).
[20] F. J. Blatt, *Physics of Electronic Conduction in Solids* (McGraw-Hill, New York, 1968), p. 446.
[21] O. E. Raichev, Phys. Rev. B **85**, 045310 (2012).
[22] V. A. Larionova and A. V. Germanenko, Phys. Rev. B **55**, 13062 (1997).
[23] X. C. Zhang, A. Pfeuffer-Jeschke, K. Ortner, V. Hock, H. Buhmann, C. R. Becker, and G. Landwehr, Phys. Rev. B **63**, 245305 (2001).
[24] E. G. Novik, A. Pfeuffer-Jeschke, T. Jungwirth, V. Latussek, C. R. Becker, G. Landwehr, H. Buhmann, and L. W. Molenkamp, Phys. Rev. B **72**, 035321 (2005).
[25] P. N. Keating, Phys. Rev. **145**, 637 (1966).
[26] J.-M. Jancu, R. Scholz, F. Beltram, and F. Bassani, Phys. Rev. B **57**, 6493 (1998).